

Speciated Measurement of Bicyclic Peroxy Radicals via Iodide-CIMS and its Implication on OH-Initiated Aromatic Oxidation

Yi Liu¹, Xin Li^{1,2*}, Ying Liu¹, Shuyu He¹, Yuqing Qiu¹, Mengdi Song¹, Jiarong Ye¹, Shengrong Lou³, Sihua Lu¹, Limin Zeng¹, Yuanhang Zhang¹

5 ¹ State Key Laboratory of Regional Environment and Sustainability, College of Environmental Sciences and Engineering, Peking University, Beijing, 100871, P.R. China.

² Collaborative Innovation Center of Atmospheric Environment and Equipment Technology, Nanjing University of Information Science & Technology, Nanjing, 210044, P.R. China.

10 ³ State Environmental Protection Key Laboratory of Formation and Prevention of Urban Air Pollution Complex, Shanghai Academy of Environmental Sciences, Shanghai 200233, P.R. China.

* Correspondence to: Xin Li (li_xin@pku.edu.cn)

Table of contents

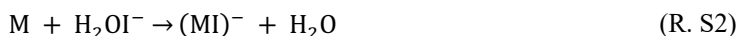
	Table S1. Calibration System: experimental conditions of aromatic-RO ₂ calibrations.	10
	Table S2. Instrumentations in this study.	10
15	Table S3. Theoretical sensitivity of Vocus AIM and traditional I-CIMS.	10
	Table S4. Information of aromatics and their tracer products detected by Vocus AIM (I-CIMS).	11
	Table S5. Information of aromatics and their tracer products detected by Vocus PTR.	11
	Table S6. Wall accommodation coefficients and wall loss rates of aromatic precursors and major tracer products.	13
	Table S7. Calibration System: branching ratios of different reaction pathways in calibrations.	14
20	Table S8. Oxidation Flow Reactor: branching ratios of different reaction pathways in toluene oxidation.	15
	Table S9. Oxidation Flow Reactor: branching ratios of different reaction pathways in m-xylene oxidation.	15
	Table S10. Measurement uncertainty contributions in tol-BPRs calibration.	16
	Table S11. Measurement uncertainty contributions in m-xyl-BPRs calibration.	17
	Scheme S1. Chemical mechanism for toluene-OH oxidation.	18
25	Scheme S2. Chemical mechanism for m-xylene-OH oxidation.	19
	Figure S1. Calibration results for Vocus AIM in this study.	20
	Figure S2 Relationship between the sensitivities and the corresponding dV ₅₀ values of standards in the AIM-CIMS (left). dV ₅₀ -based segmented linear fitting of the sensitivity and the product of the square root of m/z and fragmentation ratio (right).	20
	Figure S3 Relationship between relative transmission efficiencies of ions and their mass-to-charge ratios (m/z).	21
30	Figure S4 Comparison of calculated and measured sensitivities for different classes of compounds.	21
	Figure S5 Calibration of the sensitivity of HO ₂ radical by Vocus AIM	22
	*: The concentration of HO ₂ radicals was quantitatively determined utilizing LIF. Details about this instrument can be found in the previous reference(Wang et al., 2021).	22

	Figure S6 Sampling loss assessment in PFA line (referenced to the signal at a line length of 0.1 m.	22
35	Figure S7 Comparison of RO ₂ concentration in the calibrated system estimated using two methods in the oxidation of (left) toluene and (right) m-xylene.	23

Section S1. Iodide Chemical Ionization Time-of-Flight Mass Spectrometry with an AIM Reactor (Vocus AIM)

S1.1 Iodide Adduct Chemical Ionization

40 Vocus AIM supports various reagent ions of both positive and negative polarity. In this work, we chose iodide ions (I^-) as reagent ions. I^- is known for its remarkable sensitivity toward compounds containing a hydroxy group, which forms an adduct with I^- through a hydrogen bond, resulting in minimal fragmentation (Lee et al., 2014). Therefore, I^- has been applied in the measurement of oxidation products containing hydroxyl groups with semi-/low-volatility (He et al., 2024; He et al., 2023; Berndt et al., 2019; Wang et al., 2018; Zhao et al., 2018). Reaction S1 and Reaction S2 imply that compounds with hydroxy groups as M always forms an adduct $M+127$ with I^- through a hydrogen bond,



Owing to the lower-energy ionization reaction, the fragmentation of the iodide adduct is limited. This was confirmed by calibration results in our previous work, which showed that I^- -CIMS exhibited minimal fragmentation for the majority of the examined standards (He et al., 2024; He et al., 2023). Therefore, the fragmentation of RO_2 radicals in this work was not considered, and the iodide adducts of RO_2 radicals were assumed to be detected at $m/z (M)+127$. We identified $C_xH_{2y+1}O_2I^-$ as
50 the type of iodide adduct produced from RO_2 radicals, as they always contain an odd number of hydrogen atoms. And we attributed the observed $C_7H_9O_5I^-$ signal at m/z 300 solely to the bicyclic peroxide radicals (BPRs) from toluene. Similarly, the BPRs formed from the oxidation of xylene was identified as $C_8H_{11}O_5I^-$ at m/z 314.

S1.2 Theoretical Maximum Sensitivity

For adduct ionization, sensitivity toward a certain species is influenced by two main factors: the formation rate of product ions,
55 governed by collision frequency and the available energy in the reactor, and the transmission efficiency of these product ions to the detector, as described in Eq. 1. However, it is difficult to determine the parameters in the equation to obtain the theoretical sensitivity with calibration experiments.

Here, we used Eq. S1 to describe theoretical maximum sensitivity (S_{max}) of CIMS (Isaacman-Vanwertz et al., 2018). In the Eq. S1, reagent ions interact with sample gas in IMR and the reaction are assumed to collide at a rate, k_{coll} , of $1 \times 10^{-9} \text{ cm}^3$
60 $\text{molecular}^{-1} \text{ s}^{-1}$:

$$S_{max} = \frac{[M]_{IMR} \times f \times k_{coll} \times t_{IMR}}{10^6} \text{ (ncps/pptv)} \quad (Eq. S1)$$

where $[M]_{IMR}$ is the total concentration of gas molecules in IMR, f is the ratio of concentrations of gas molecules in sample to that in IMR, so $f = 0.88$ in Vocus AIM and t_{IMR} is the residence time of the IMR.

In Vocus AIM, the reagent ions at a flow rate of 250 sccm were mixed with sample gas at a flow rate of 2 slpm in the IMR with a volume of about 45 cm^3 (V_{IMR}). Under the optimized conditions of the IMR, the pressure (P_{actual}) was 70 mbar and the

65 temperature (T_{actual}) was 45°C. The gas flow rate (Q_{IMR}) and the residence time can be calculated Eq. S2 and Eq. S3, respectively:

$$Q_{IMR} = \frac{P_0 Q_0}{T_0} \times \frac{T_{actual}}{P_{actual}} \quad (\text{Eq. S2})$$

$$t_{IMR} = \frac{V_{IMR}}{Q_{IMR}} \quad (\text{Eq. S3})$$

where P_0 and T_0 are the normal pressure and temperature, and Q_0 is the flow rate of sample gas and reagent ions. Table S3 presents the theoretical sensitivity of the Vocus AIM, which was estimated about 112 ncps/pptv. Our calibration results (Figure S1) indicate that the molecular-ion reaction efficiency in Vocus AIM, calculated via Eq. S4, reached a maximum of approximately 30% for 4-nitrophenol ($C_6H_5NO_3$).

$$reaction\ efficiency = \frac{S_{calibration}}{S_{max}} \quad (\text{Eq. S4})$$

S1.3 Calibration and Quantification

A total of 32 standards were calibrated using permeation tubes and liquid-solution-based techniques for Vocus AIM. These standards can be classified into 5 categories, namely acids (mono-, di- acids), phenols/alcohols (mono-, di- and poly-phenols/alcohols), carbonyl-acids, hydroxyl-acids and nitrophenols. As the Figure S1, the instrumental sensitivities varied between chemicals, with the orders of magnitude ranging from 10^{-1} to 10^2 ncps/pptv. For other uncalibrated compounds, an empirical approach based on half of the iodide adducts dissociate (dV_{50}), was developed for I-CIMS to extrapolate the instrumental sensitivities according to our previous studies (He et al., 2024; He et al., 2023).

The sensitivities of 28 authentic standards and corresponding dV_{50} obtained in our I-CIMS system are plotted in Figure S2. As noted in previous studies, deviations between the observed sensitivities and the values predicted by the log-linear trend may primarily result from the limitations of dV_{50} in accurately reflecting the effective formation rates of ion-molecule clusters (Lopez-Hilfiker et al., 2016). He et al. proposed a method to estimated sensitivities by considering the ion-molecule cluster formation in the IMR region as a function of dV_{50} , mass-dependent transmission efficiency (TR), and collision-induced decomposition fraction (f) prior to detection (He et al., 2024), as expressed in Eq. S5.

$$S_i = \int_0^t k_f (dV_{50}^i) [I^-] dt \times TR_i \left(\frac{m}{z} \right) \times f_i \quad (\text{Eq. S5})$$

The effective formation rate of ion-molecule reactions is generally influenced by the chemical functionality and steric configuration of the target molecule (Lee et al., 2014). In this study, calibrating species were classified into groups based on their dV_{50} values, with each group spanning 1 V (Figure S2). It was assumed that within each category, the formation rate of ion-molecule clusters remained relatively consistent. As depicted in Figure S2, compounds with dV_{50} below 3 V were categorized as the first group, most of which contained a single polar functional group like monoacids. The second group, with dV_{50} values between 3 and 4 V, primarily included compounds with two or more identical hydroxyl or carboxylic groups, such

90 as diacids and di-/poly-alcohols or phenols. Compounds with dV_{50} values exceeding 4 V were grouped into the third category, which included most nitro-phenols/alcohols and certain hydroxy-acids. These compounds exhibited enhanced hydrogen-bonding capabilities, increasing their interaction efficiency with I⁻. Linear regression analyses were performed for each dV_{50} subgroup to correlate the observed sensitivities of standards with the product of the square root of m/z and fragmentation ratio ($\sqrt{m/z} \times f$), where f was derived from the fragmentation patterns of the calibrating standards or collision cross-sections from
95 previous research (Zhang et al., 2016; He et al., 2024). The sensitivities calculated via linear fitting showed strong agreement with the measured values for authentic standards, with uncertainties mostly below 40%. For uncalibrated species, the estimated sensitivities using the segmented fitting approach in I⁻-CIMS had uncertainties ranging from approximately 15% to 35%, as listed in Table S10, S11.

S1.4 Estimations of Binding Energy

100 We used the ORCA version 5.0.4 to calculate the binding energies of iodide adducts of BPRs and standards, including formic acid (CH₂O₂), 2,4-dihydroxytoluene (C₇H₈O₂), 4-nitrophenol (C₆H₅NO₃), 2-methyl-6-nitrophenol (C₇H₇NO₃) and pinonic acid (C₁₀H₁₆O₃). Geometry optimizations and frequency analyses were performed at the B3LYP/ma-def2-TZVP(-f) level with Grimme's D3 dispersion correction, using VeryTightOpt convergence criteria, a maximum of 1000 SCF iterations (VeryTightSCF), DefGrid3 integration grids, and AutoAux-generated auxiliary basis sets for RI acceleration. Single-point
105 energies were computed on the optimized geometries at the DLPNO-CCSD(T)/aug-cc-pVQZ level with TightPNO truncation, VeryTightSCF convergence settings, and the aug-cc-pVQZ/C auxiliary basis sets (with the corresponding ECPs) for RI-JK and RI-MP2 integrals.

Section S2. Other Relevant Instrumentations

S2.1 Proton Transfer Reaction Time-of-Flight Mass Spectrometry (PTR-MS)

110 Aromatic precursors and some gas-phase products were measured using a ToFwerk Vocus proton transfer reaction (PTR) time-of-flight mass spectrometer with a mass resolution of ~10,000. PTR-MS was operated at the pressure of 2.1 mbar in drift tube, applying a voltage of 630 V to achieve an E/N ratio (electric field strength to gas number density) of 120Td, so as to strike a balance between the formation of hydronium water clusters and the fragmentation of product ions. The drift tube was maintained at 100°C, to largely prevent vapor deposition to the wall.
115 In this study, comprehensive calibrations were performed using a total of 43 representative standards, encompassing volatile organic compounds (VOCs) and intermediate/semi-volatile organic compounds (I/SVOCs) with different functional groups. These standards included hydrocarbons, aldehydes, ketones, alcohols/phenols, carboxylic acids, and furans. Calibrations were performed at 5–6 different concentration levels (from 0.2 to several ppbv), and the sensitivities were determined by the fitting

120 slopes between instrument signals and the corresponding concentrations, yielding fit values with R^2 ranging from 0.9990 to 0.9999.

For uncalibrated compounds without authentic standards, theoretical sensitivities can be estimated based on the transmission efficiency and proton-transfer reaction rate, as described in our earlier studies (He et al., 2024; He et al., 2023). The response factor of a compound can be expressed by the following Eq. S6.

$$S_{[R]} = \frac{N \times k \times t_R}{10^9} \times \frac{TR_{RH^+}}{TR_{H_3O^+}} \times f \times 10^6 \quad (\text{Eq. S6})$$

125 $[R]$ is the response factor of compound R in Vocus PTR, which was defined as the ion signal of target compound at a volume mixing ratio of ppbv. N is the number of air molecules in the drift tube, expressed in unit of molecule/cm³, k is the rate constant of proton-transfer reaction, t_R refers to the reaction time in the drift tube, and f means the fragmentation fraction. TR_{RH^+} and $TR_{H_3O^+}$ are the ion transmission efficiencies for RH^+ and H_3O^+ , respectively. The values of N and t_R can be calculated by working parameters of drift tube.

130 Ion transmission efficiency in TOF-MS is known to be proportional to the square root of the mass-to-charge ratio (m/z) (Yuan et al., 2017). In this study, we used an empirical expression relating ion transmission efficiency to m/z , as shown in Figure S3, based on existing standards with minimal fragmentation in Vocus PTR. To validate this approach, we compared the calculated response factors with the measured values for different compounds (Figure S4). The results indicated that the calculated response factors were in good agreement with the measured ones, with absolute deviations below 15% (accounting for the fragmentation fraction based on the mass spectra of different compounds). Therefore, we conclude that this method is reliable for estimating the response factors of target oxidation products in the absence of standards.

135 Uncertainty for the calibrated species was within 10%. For the aromatic oxidation products not calibrated in this study, the uncertainty was anticipated to be higher due to the effects of transmission and fragmentation. The transmission uncertainty for uncalibrated products was quantified by an upper limit of 15% for the relative deviations between the measured and estimated sensitivities of calibrated compounds exhibiting minimal fragmentation (as illustrated in Figure S4). The fragmentation uncertainties for uncalibrated products were determined by comparing the relative deviations in the fragmentation patterns of calibrated compounds with chemically similar structures (He et al., 2024; He et al., 2023). Consequently, the overall uncertainty for uncalibrated products ranged from 15% to 25%, as listed in Table S10, S11.

S2.2 Traditional Iodide Chemical Ionization Time-of-Flight Mass Spectrometry (Traditional I-CIMS)

145 Conventional I-CIMS instruments (Aerodyne Research Inc.) were employed for comparative analysis with the Vocus AIM in detecting RO_2 radicals. The iodide reagent ions (I^-) were generated by flowing ultra-high purity nitrogen at 2 slpm, doped with methyl iodide, through an X-ray ionization source connected to IMR. A sample flow of 2.3 slpm was introduced into the IMR, where it mixed with the I^- reagent ion stream to facilitate molecular-ion formation. The instrument demonstrated a mass resolution of $\sim 5,000$ at 100–500 Th and a total ion count of $\sim 20,000$ cps.

A total of 54 standards were calibrated using permeation tubes and liquid-solution based techniques. The instrumental sensitivities varied between chemicals, with the orders of magnitude ranging from 10^{-2} to 10^2 ncps/pptv, which has been described in detail in our previous work (He et al., 2023). Similarly, we estimated the molecular-ion reaction efficiency in traditional I-CIMS via Eq. S4 and it reached a maximum of approximately 10% for 4-nitrophenol ($C_6H_5NO_3$) as Table S3 shows.

S2.3 Others

NO_x, temperature and relative humidity were monitored by the chemiluminescence analyzer (Model 42i-TL, Thermo Fisher Scientific, USA) and a temperature and humidity sensor. Besides, a laser-induced fluorescence system was used when we calibrated the sensitivity of HO₂ radicals in Vocus AIM. More details are shown in Table S2.

Section S3. Wall Loss in the Experimental Systems

The wall-induced decay of products from aromatic oxidation was taken into consideration in this study. This process can be described by the first-order reaction kinetic, and the corresponding rate coefficient is expressed as Equation S7 (Zhang et al., 2015; McMurry and Grosjean, 1985).

$$k_{w,i} = \frac{A}{V} \times \frac{\frac{\alpha_{w,i} \bar{v}_i}{4}}{\frac{\pi}{2} \times \frac{\alpha_{w,i} \bar{v}_i}{4\sqrt{D_i K_e}} + 1} \quad (\text{Eq. S7})$$

where the $k_{w,i}$ is the wall loss rate constant of compound i . A/V is the ratio of surface to volume of the tube (40 m^{-1} for the calibration system and 20 m^{-1} for the Oxidation Flow Reactor in this study). $\alpha_{w,i}$ is the mass accommodation coefficient. \bar{v}_i is the mean thermal speed of molecule i , related to the temperature and molecular weight, and can be calculated by the Equation S14. D_i and K_e refer to the molecular diffusion coefficient and eddy diffusion coefficient, respectively. D_i in Equation S8 can be calculated by the Equation S9.

$$\bar{v}_i = \sqrt{\frac{8RT}{\pi MW_i}} \quad (\text{Eq. S8})$$

$$D_i = D_{CO_2} \times \frac{MW_{CO_2}}{MW_i} \quad (\text{Eq. S9})$$

where R represents the ideal gas constant, T the temperature during the experiments, MW_i the molecular weight of compound i , D_{CO_2} the molecular diffusion coefficient of CO₂ ($1.38 \times 10^{-5} \text{ m}^2/\text{s}$), and MW_{CO_2} the molecular weight of CO₂. K_e characterized the capacity of turbulent mixing in the reactor. Some estimated values have been given by empirical fittings. For instance, McMurry and Grosjean recommended the K_e values to be 0.12 s^{-1} and 0.02 s^{-1} for 60 m^3 and 4 m^3 chamber (McMurry and Grosjean, 1985), respectively. Besides, Zhang et al. proposed the smaller K_e value of 0.015 s^{-1} for their 28 m^3

chamber (Zhang et al., 2015), considering the not active mixing. In this study, 0.0042s^{-1} was adopted due to the nearly equivalent volume in this study compare to the previous research (Huang et al., 2018).

The last unknown parameter $\alpha_{w,i}$, representing the fraction of deposited molecules when encountering the wall, is dependent on the molecular property of compound i in theory. Specifically, vapors with lower volatility are more likely to deposit on the wall (He et al., 2023). Therefore, previous study (Zhang et al., 2015) proposed a set of optimized empirical equations that related $\alpha_{w,i}$ to the number of carbon and oxygen atoms contained in the compounds through volatility, as the Equation S10 and S11 shown. That meant $\alpha_{w,i}$ can be estimated from the chemical composition of the target compounds.

$$\log_{10} \alpha_{w,i} = -0.1919 \times \log_{10} C_i^* - 6.32 \quad (\text{Eq. S10})$$

$$\log_{10} C_i^* = (n_C^0 - n_C^i)b_C - n_O^i b_O - 2 \frac{n_C^i n_O^i}{n_C^i + n_O^i} b_{CO} \quad (\text{Eq. S11})$$

where C_i^* is the saturation vapor concentration, which can be calculated based on the group-contribution method proposed in the previous study (Nannoolal et al., 2009). n_C^0 is the number of carbon atoms of $1 \mu\text{g}/\text{m}^3$ alkane, b_C , b_O and b_{CO} represent the interaction between carbon-carbon atoms, oxygen-oxygen atoms and carbon-oxygen atoms, respectively. Those four parameters have been determined by Zhang et al (2015), where species were employed to obtain the optimal fitting. The remaining n_C^i and n_O^i refer to the number of carbon and oxygen atoms in the target molecule i , respectively. $\alpha_{w,i}$ of the aromatic precursors and major tracer products in this study are listed in Table S6.

References

- Berndt, T., Hyttinen, N., Herrmann, H., and Hansel, A.: First oxidation products from the reaction of hydroxyl radicals with isoprene for pristine environmental conditions, *Commun Chem*, 2, ARTN 21 10.1038/s42004-019-0120-9, 2019.
- Galloway, M. M., Huisman, A. J., Yee, L. D., Chan, A. W. H., Loza, C. L., Seinfeld, J. H., and Keutsch, F. N.: Yields of oxidized volatile organic compounds during the OH radical initiated oxidation of isoprene, methyl vinyl ketone, and methacrolein under high-NO conditions, *Atmos Chem Phys*, 11, 10779-10790, 10.5194/acp-11-10779-2011, 2011.
- He, S. Y., Liu, Y., Song, M. D., Li, X., Lu, S. H., Chen, T. Z., Mu, Y. J., Lou, S. R., Shi, X. D., Qiu, X. H., Zhu, T., and Zhang, Y. H.: Insights into the Peroxide-Bicyclic Intermediate Pathway of Aromatic Photooxidation: Experimental Yields and NOx-Dependency of Ring-Opening and Ring-Retaining Products, *Environ Sci Technol*, 57, 20657-20668, 10.1021/acs.est.3c05304, 2023.
- He, S. Y., Liu, Y., Song, M. D., Li, X., Lou, S. R., Ye, C. S., Liu, Y. J., Liu, Y., Ye, J. R., Lu, S. H., Zhou, W. X., Qiu, X. H., Zhu, T., and Zeng, L. M.: Empirical Approach to Quantifying Sensitivity in Different Chemical Ionization Techniques for Organonitrates and Nitroaromatics Constrained by Ion-Molecule Reaction and Transmission Efficiency, *Anal Chem*, 96, 16882-16890, 10.1021/acs.analchem.4c03751, 2024.

- 200 Huang, Y. L., Zhao, R., Charan, S. M., Kenseth, C. M., Zhang, X., and Seinfeld, J. H.: Unified Theory of Vapor-Wall Mass Transport in Teflon-Walled Environmental Chambers, *Environ. Sci. Technol.*, 52, 2134-2142, 10.1021/acs.est.7b05575, 2018.
- Isaacman-VanWertz, G., Massoli, P., O'Brien, R., Lim, C., Franklin, J. P., Moss, J. A., Hunter, J. F., Nowak, J. B., Canagaratna, M. R., Misztal, P. K., Arata, C., Roscioli, J. R., Herndon, S. T., Onasch, T. B., Lambe, A. T., Jayne, J. T., Su, L. P., Knopf, D. A., Goldstein, A. H., Worsnop, D. R., and Kroll, J. H.: Chemical evolution of atmospheric organic carbon over multiple
205 generations of oxidation, *Nat Chem*, 10, 462-468, 10.1038/s41557-018-0002-2, 2018.
- Lee, B. H., Lopez-Hilfiker, F. D., Mohr, C., Kurtén, T., Worsnop, D. R., and Thornton, J. A.: An Iodide-Adduct High-Resolution Time-of-Flight Chemical-Ionization Mass Spectrometer: Application to Atmospheric Inorganic and Organic Compounds, *Environ Sci Technol*, 48, 6309-6317, 10.1021/es500362a, 2014.
- Lopez-Hilfiker, F. D., Iyer, S., Mohr, C., Lee, B. H., D'Ambro, E. L., Kurtén, T., and Thornton, J. A.: Constraining the
210 sensitivity of iodide adduct chemical ionization mass spectrometry to multifunctional organic molecules using the collision limit and thermodynamic stability of iodide ion adducts, *Atmos Meas Tech*, 9, 1505-1512, 10.5194/amt-9-1505-2016, 2016.
- McMurry, P. H. and Grosjean, D.: Gas and Aerosol Wall Losses in Teflon Film Smog Chambers, *Environ Sci Technol*, 19, 1176-1182, DOI 10.1021/es00142a006, 1985.
- Nannoolal, Y., Rarey, J., and Ramjugernath, D.: Estimation of pure component properties. Part 4: Estimation of the saturated
215 liquid viscosity of non-electrolyte organic compounds via group contributions and group interactions, *Fluid Phase Equilibr*, 281, 97-119, 10.1016/j.fluid.2009.02.016, 2009.
- Wang, S. N., Riva, M., Yan, C., Ehn, M., and Wang, L. M.: Primary Formation of Highly Oxidized Multifunctional Products in the OH-Initiated Oxidation of Isoprene: A Combined Theoretical and Experimental Study, *Environ Sci Technol*, 52, 12255-12264, 10.1021/acs.est.8b02783, 2018.
- 220 Xu, L., Moller, K. H., Crounse, J. D., Kjaergaard, H. G., and Wennberg, P. O.: New Insights into the Radical Chemistry and Product Distribution in the OH-Initiated Oxidation of Benzene, *Environ Sci Technol*, 54, 13467-13477, 10.1021/acs.est.0c04780, 2020.
- Yuan, B., Koss, A. R., Warneke, C., Coggon, M., Sekimoto, K., and de Gouw, J. A.: Proton-Transfer-Reaction Mass Spectrometry: Applications in Atmospheric Sciences, *Chem Rev*, 117, 13187-13229, 10.1021/acs.chemrev.7b00325, 2017.
- 225 Zhang, X., Schwantes, R. H., McVay, R. C., Lignell, H., Coggon, M. M., Flagan, R. C., and Seinfeld, J. H.: Vapor wall deposition in Teflon chambers, *Atmos Chem Phys*, 15, 4197-4214, 10.5194/acp-15-4197-2015, 2015.
- Zhang, X., Krechmer, J. E., Groessl, M., Xu, W., Graf, S., Cubison, M., Jayne, J. T., Jimenez, J. L., Worsnop, D. R., and Canagaratna, M. R.: A novel framework for molecular characterization of atmospherically relevant organic compounds based on collision cross section and mass-to-charge ratio, *Atmos. Chem. Phys.*, 16, 12945-12959, 10.5194/acp-16-12945-2016, 2016.
- 230 Zhao, Y., Thornton, J. A., and Pye, H. O. T.: Quantitative constraints on autoxidation and dimer formation from direct probing of monoterpene-derived peroxy radical chemistry, *P Natl Acad Sci USA*, 115, 12142-12147, 10.1073/pnas.1812147115, 2018.

Table S1. Calibration System: experimental conditions of aromatic-RO₂ calibrations.

Expt NO.	Reactants	Temperature [°C]	Relative Humidity [%]	OH _{av} [molecule/cm ³]
1	5ppb TOL	25±1	40±5	1.43×10 ¹⁰
2	10ppb TOL	25±1	40±5	1.46×10 ¹⁰
3	15ppb TOL	25±1	40±5	1.23×10 ¹⁰
4	20ppb TOL	25±1	40±5	1.23×10 ¹⁰
5	10ppb m-XYL	25±1	40±5	5.50×10 ⁹
6	15ppb m-XYL	25±1	40±5	5.31×10 ⁹
7	20ppb m-XYL	25±1	40±5	6.10×10 ⁹
8	25ppb m-XYL	25±1	40±5	6.31×10 ⁹

*The calibrations were conducted under essentially fixed low-NO_x (~0.5 ppbv) and high-HO₂ (~10¹¹ molecular/cm³) conditions, by adjusting the precursor concentration to vary the NO/precursor ratio, to determine whether RO₂ radicals can proceed linearly.

Table S2. Instrumentations in this study.

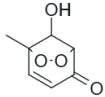
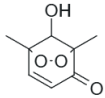
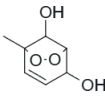
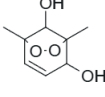
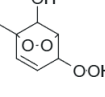
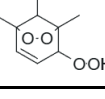
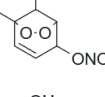
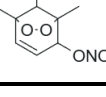
Instrument	Detection limit	Time resolution	Sampling flow rate
Vocus AIM (Tofwerk, Switzerland)	~pptv	1s	~2L/min
Vocus PTR (Tofwerk, Switzerland)	~pptv	1s	~100mL/min
NO _x analyzer (Model 42i-TL, Thermo Fisher Scientific, USA)	~100pptv	1min	~1L/min
HO _x -LIF (Wang et al., 2021)*	~0.1pptv	1min	~2L/min

*: The calibration of Vocus AIM for HO₂ is performed utilizing the LIF (Laser-Induced Fluorescence) instrumentation at Anhui Institute of Optics and Fine Mechanics. The calibration results are listed in Figure S5.

Table S3. Theoretical sensitivity of Vocus AIM and traditional I-CIMS.

	Vocus AIM	Traditional I-CIMS(He et al., 2023)
P_{actual}	70 mbar	380 mbar
T_{actual}	45°C	30°C
Q_{all}	2.25 L/min	4 L/min
V_{IMR}	~45 cm ³	~47 cm ³
$[M]_{IMR}$	1.59×10 ¹⁸ molecules/cm ³	9.08×10 ¹⁸ molecules/cm ³
f	0.88	0.5
t_{IMR}	0.08	0.24
S_{max}	112 ncps/pptv	1090 ncps/pptv
Sen. for C ₆ H ₅ NO ₃	37 ncps/pptv	66 cps/pptv

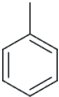
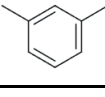
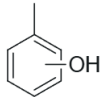
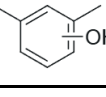
Table S4. Information of aromatics and their tracer products detected by Vocus AIM (F-CIMS).

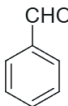
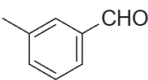
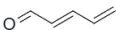
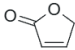
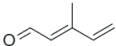
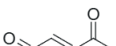
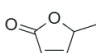
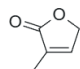
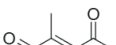
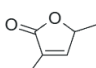
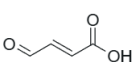
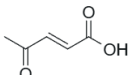
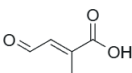
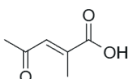
Class	Formula	Ion mass [amu]	Compound	Structure	Sensitivity [ncps/pptv]
1 ^e	C ₇ H ₈ O ₄	157.05	Bicyclic carbonyl		7.8
	C ₈ H ₁₀ O ₄	171.07	Bicyclic carbonyl		8.7
2 ^e	C ₇ H ₁₀ O ₄	159.06	Bicyclic alcohol		9.8
	C ₈ H ₁₂ O ₄	173.08	Bicyclic alcohol		10.7
3 ^e	C ₇ H ₁₀ O ₅	175.05	Bicyclic hydroperoxide		11.4
	C ₈ H ₁₂ O ₅	189.07	Bicyclic hydroperoxide		14.3
4 ^e	C ₇ H ₉ NO ₆	186.04	Bicyclic nitrate		18
	C ₈ H ₁₁ NO ₆	218.07	Bicyclic nitrate		20.1

^e Ring-retaining products from peroxide-bicyclic intermediate pathway.

* Sensitivity was obtained from calibration.

Table S5. Information of aromatics and their tracer products detected by Vocus PTR.

Class	Formula	Ion mass [amu]	Compound	Structure	Sensitivity [cps/ppbv]
1 ^a	C ₇ H ₈	93.07	Toluene		14766
	C ₈ H ₁₀	107.09	m-Xylene		17280
2 ^b	C ₇ H ₈ O	109.06	Cresol		17797
	C ₈ H ₁₀ O	123.08	2,6-Dimethylphenol		18103

3 ^c	C ₇ H ₆ O	107/05	Benzaldehyde		11891
	C ₈ H ₈ O	121.06	3-Methylbenzaldehyde		11443
4 ^d	C ₄ H ₄ O ₂	85/03	Butene dial		17604
	C ₄ H ₄ O ₂	85.03	2(5H)-Furanone		9929
	C ₅ H ₆ O ₂	99.04	2-Methylbutenedial		18169
	C ₅ H ₆ O ₂	99.04	4-Oxo-2-pentenal		18169
	C ₅ H ₆ O ₂	99.04	5-Methyl-2(5H)-furanone		10223
	C ₅ H ₆ O ₂	99.04	3-Methyl-2(5H)-furanone		10223
	C ₆ H ₈ O ₂	113.06	Methyl-4-oxo-2-pentenal		18489
	C ₆ H ₈ O ₂	113.06	3,5-Dimethyl-2(5H)-furanone		10734
	C ₄ H ₄ O ₃	101.02	Male aldehydic acid		10741
	C ₅ H ₆ O ₃	115.04	4-Oxo-pent-2-enoic acid		11826
	C ₅ H ₆ O ₃	115.04	2-Methyl-4-oxobut-2-enoic acid		11826
	C ₆ H ₈ O ₃	129.05	Acetyl methacrylic acid		12101

a Aromatic precursors.

b Ring-retaining products from phenolic pathway.

c Ring-retaining products from benzaldehyde pathway.

d Ring-opening products from peroxide-bicyclic intermediate pathway.

* Sensitivity was obtained from calibration.

Table S6. Wall accommodation coefficients and wall loss rates of aromatic precursors and major tracer products.

NO.	Formula	Wall accommodation coefficient (α_w)	Wall loss rate (k_w , s ⁻¹)
1	C ₇ H ₈	1.14×10^{-8}	9.39×10^{-7}
2	C ₈ H ₁₀	1.37×10^{-8}	1.05×10^{-6}
3	C ₇ H ₈ O	2.23×10^{-8}	1.70×10^{-6}
4	C ₇ H ₆ O	2.23×10^{-8}	1.71×10^{-6}
5	C ₈ H ₁₀ O	2.65×10^{-8}	1.90×10^{-6}
6	C ₈ H ₈ O	2.65×10^{-8}	1.91×10^{-6}
8	C ₄ H ₄ O ₂	3.03×10^{-8}	2.61×10^{-6}
9	C ₅ H ₆ O ₂	3.48×10^{-8}	2.78×10^{-6}
10	C ₆ H ₈ O ₂	4.03×10^{-8}	3.01×10^{-6}
11	C ₄ H ₄ O ₃	7.26×10^{-8}	5.73×10^{-6}
12	C ₅ H ₆ O ₃	8.10×10^{-8}	5.99×10^{-6}
13	C ₆ H ₈ O ₃	9.19×10^{-8}	6.41×10^{-6}
14	C ₇ H ₈ O ₄	2.45×10^{-7}	1.55×10^{-5}
15	C ₈ H ₁₀ O ₄	2.42×10^{-7}	1.17×10^{-5}
16	C ₇ H ₁₀ O ₄	2.45×10^{-7}	1.54×10^{-5}
17	C ₈ H ₁₂ O ₄	2.42×10^{-7}	1.17×10^{-5}
18	C ₇ H ₁₀ O ₅	2.45×10^{-7}	1.46×10^{-5}
19	C ₈ H ₁₂ O ₅	2.42×10^{-7}	1.12×10^{-5}
20	C ₇ H ₉ O ₅	2.53×10^{-5}	1.47×10^{-3}
21	C ₈ H ₁₁ O ₅	2.48×10^{-5}	1.46×10^{-3}

Table S7. Calibration System: branching ratios of different reaction pathways in calibrations.

Aromatic precursor	Conditions	Branching ratios of different reaction pathways (%)									
		Benzaldehyde pathway	Phenolic pathway	Peroxide-bicyclic intermediate pathway							
	NO/TOL	C ₇ H ₆ O	C ₇ H ₈ O	C ₄ H ₄ O ₂	C ₅ H ₆ O ₂	C ₄ H ₄ O ₃	C ₅ H ₆ O ₃	C ₇ H ₈ O ₄	C ₇ H ₁₀ O ₄	C ₇ H ₁₀ O ₅	SUM
TOL	0.08	5.3	18.4	4.7	9.7	3.9	2.1	23	3.2	21.9	68.5
	0.04	5.4	18.4	4.6	9.1	4	1.7	23.1	3.6	21.8	67.9
	0.03	5.4	18.8	4.9	8.6	4	1.7	22.4	3.5	21.8	66.9
	0.02	5.4	18.9	4.6	8.2	3.8	1.9	22.9	3.5	22	66.9
	NO/m-XYL	C ₈ H ₈ O	C ₈ H ₁₀ O	C ₅ H ₆ O ₂	C ₆ H ₈ O ₂	C ₅ H ₆ O ₃	C ₆ H ₈ O ₃	C ₈ H ₁₀ O ₄	C ₈ H ₁₂ O ₄	C ₈ H ₁₂ O ₅	SUM
m-XYL	0.1	2.8	8.8	23.5	6.0	3.2	1.5	24.7	5.7	21.5	86.1
	0.08	2.8	8.8	23.3	5.9	3.2	2.2	24.4	5.9	21.0	85.9
	0.04	3.1	8.9	23.0	6.4	3.4	3.0	23.0	5.6	21.2	85.6
	0.02	3.1	8.8	23.6	6.3	3.4	2.7	23.0	5.8	21.1	85.9

Table S8. Oxidation Flow Reactor: branching ratios of different reaction pathways in toluene oxidation.

Aromatic precursor	Conditions	Branching ratios of different reaction pathways (%)									
		Benzaldehyde pathway	Phenolic pathway	Peroxide-bicyclic intermediate pathway							
				Product-yield method						Direct-measured method	
	NO/TOL	C ₇ H ₆ O	C ₇ H ₈ O	C ₄ H ₄ O ₂	C ₅ H ₆ O ₂	C ₄ H ₄ O ₃	C ₅ H ₆ O ₃	C ₇ H ₈ O ₄	C ₇ H ₁₀ O ₄	C ₇ H ₁₀ O ₅	C ₇ H ₉ O ₅
TOL	0.03	11.7	20.9	6.1	26.2	2.2	2.3	4.4	0.6	3.2	55.3
	0.04	11.3	21.2	6.1	26.6	2.2	2.4	4.6	0.8	3.4	56.2
	0.06	11.3	22.6	6.5	28.6	2.2	2.7	5.0	0.6	3.7	58.7
	0.1	10.3	22.2	6.5	29.4	2.0	2.8	5.3	0.8	4.0	58.8
	0.2	9.4	22.3	7.5	30.8	2.0	3.4	6.4	1.1	4.8	64.1

Table S9. Oxidation Flow Reactor: branching ratios of different reaction pathways in m-xylene oxidation.

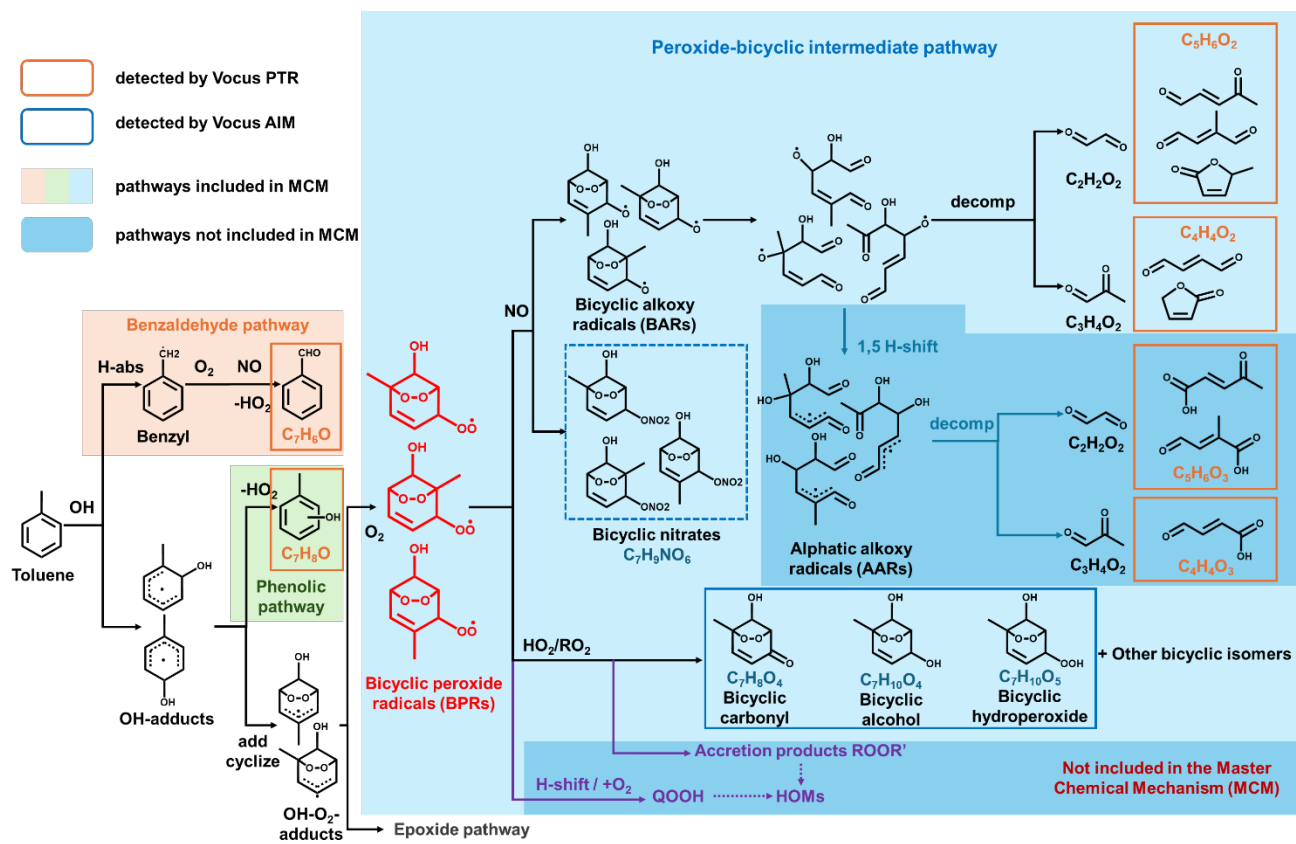
Aromatic precursor	Conditions	Branching ratios of different reaction pathways (%)									
		Benzaldehy de pathway	Phenolic pathway	Peroxide-bicyclic intermediate pathway							
				Product-yield method						Direct-measured method	
	NO/m-XYL	C ₈ H ₈ O	C ₈ H ₁₀ O	C ₅ H ₆ O ₂	C ₆ H ₈ O ₂	C ₅ H ₆ O ₃	C ₆ H ₈ O ₃	C ₈ H ₁₀ O ₄	C ₈ H ₁₂ O ₄	C ₈ H ₁₂ O ₅	C ₈ H ₁₁ O ₅
m-XYL	0.07	5.5	5.8	28.7	14.8	1.4	1.0	5.1	2.3	6.0	71.0
	0.09	5.3	6.0	29.9	15.8	1.4	0.7	5.5	2.3	5.9	72.1
	0.12	4.8	6.0	30.0	16.6	1.3	0.9	5.4	2.2	5.9	72.3
	0.19	4.3	6.1	30.2	18.6	1.4	0.9	5.4	2.2	5.8	72.4
	0.4	3.6	6.0	30.4	24.2	1.4	0.8	5.9	2.2	5.8	74.3

Table S10. Measurement uncertainty contributions in tol-BPRs calibration.

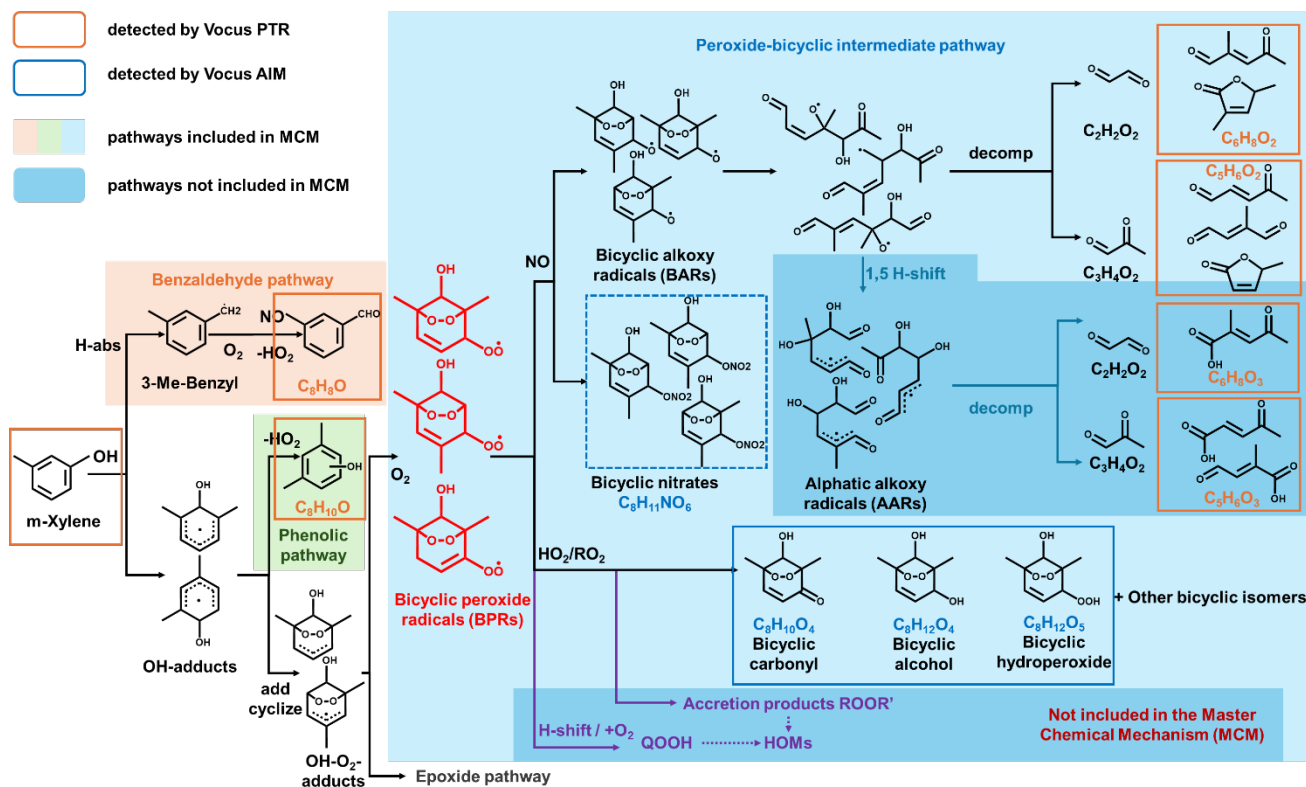
NO	Formula	Compound	Measurement uncertainty	Loss uncertainty	Total uncertainty (He et al., 2023)
			Sensitivity	Wall loss (Zhang et al., 2015)	
1	C ₇ H ₈ O	Cresol	9.50%	15%	17.76%
2	C ₇ H ₆ O	Benzaldehyde	7.60%	15%	16.82%
3	C ₇ H ₈ O ₄	Bicyclic carbonyl	22%	15%	26.63%
4	C ₇ H ₁₀ O ₄	Bicyclic alcohol	22%	15%	26.63%
5	C ₇ H ₁₀ O ₅	Bicyclic hydroperoxide	22%	15%	26.63%
6	C ₄ H ₄ O ₂	Butene dial	20%	15%	25.00%
7	C ₄ H ₄ O ₂	2(5H)-Furanone	18%	15%	23.43%
8	C ₅ H ₆ O ₂	2-Methylbutenedial	18%	15%	23.43%
9	C ₅ H ₆ O ₂	4-Oxo-2-pentenal	18%	15%	23.43%
10	C ₅ H ₆ O ₂	5-Methyl-2(5H)-furanone	16%	15%	21.93%
11	C ₅ H ₆ O ₂	3-Methyl-2(5H)-furanone	7%	15%	16.55%
12	C ₄ H ₄ O ₃	Malealdehydic acid	21%	15%	25.81%
13	C ₅ H ₆ O ₃	4-Oxo-pent-2-enoic acid	21%	15%	25.81%
14	C ₅ H ₆ O ₃	2-Methyl-4-oxobut-2-enoic acid	21%	15%	25.81%
15	The branching ratio of RO ₂ pathway, α		-	-	20.1%

Table S11. Measurement uncertainty contributions in m-xyl-BPRs calibration.

NO	Formula	Compound	Measurement uncertainty	Loss uncertainty	Total uncertainty (He et al., 2023)
			Sensitivity	Wall loss (Zhang et al., 2015)	
1	C ₈ H ₁₀ O	2,6-Dimethylphenol	10%	15%	18.03%
2	C ₈ H ₈ O	3-Mehtylbenzaldehyde	10%	15%	18.03%
3	C ₈ H ₁₀ O ₄	Bicyclic carbonyl	20%	15%	25.00%
4	C ₈ H ₁₂ O ₄	Bicyclic alcohol	20%	15%	25.00%
5	C ₈ H ₁₂ O ₅	Bicyclic hydroperoxide	20%	15%	25.00%
6	C ₅ H ₆ O ₂	2-Methylbutenedial	18%	15%	23.43%
7	C ₅ H ₆ O ₂	4-Oxo-2-pentenal	18%	15%	23.43%
8	C ₅ H ₆ O ₂	5-Methyl-2(5H)-furanone	16%	15%	21.93%
9	C ₅ H ₆ O ₂	3-Methyl-2(5H)-furanone	7%	15%	16.55%
10	C ₆ H ₈ O ₂	Methyl-4-oxo-2-pentenal	18%	15%	23.43%
11	C ₆ H ₈ O ₂	3,5-Dimethy-2(5H)-furanone	16%	15%	21.93%
12	C ₅ H ₆ O ₃	4-Oxo-pent-2-enoic acid	21%	15%	25.81%
13	C ₅ H ₆ O ₃	2-Methyl-4-oxobut-2-enoic acid	21%	15%	25.81%
14	C ₆ H ₈ O ₃	Acetyl methacrylic acid	21%	15%	25.81%
15	The branching ratio of RO ₂ pathway, α		-	-	21.0%



Scheme S1. Chemical mechanism for toluene-OH oxidation.

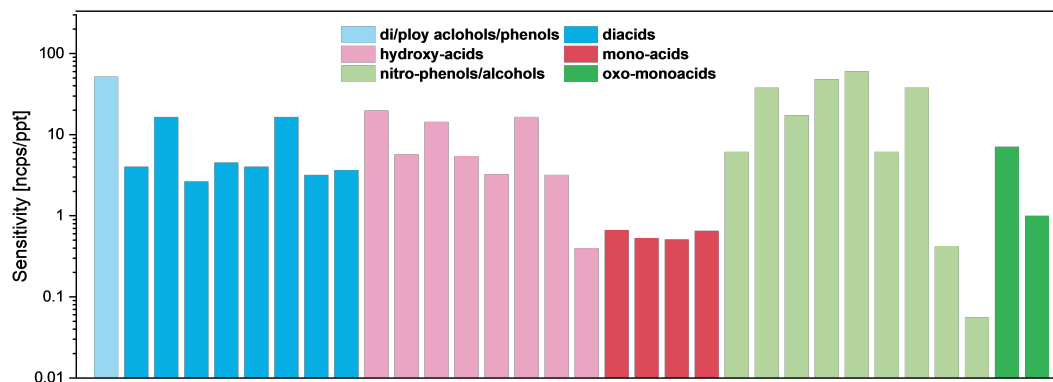


Scheme S2. Chemical mechanism for m-xylene-OH oxidation.

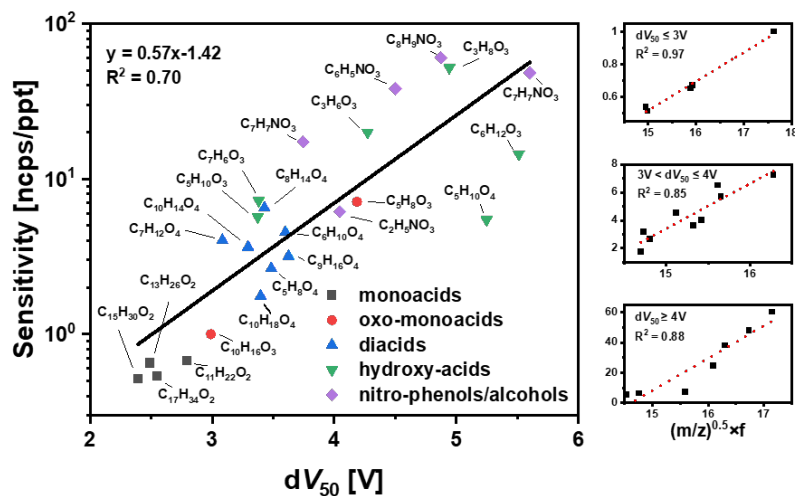
10

15

20



25 Figure S1. Calibration results for Vocus AIM in this study.



30 Figure S2 Relationship between the sensitivities and the corresponding dV_{50} values of standards in the AIM-CIMS (left). dV_{50} -based segmented linear fitting of the sensitivity and the product of the square root of m/z and fragmentation ratio (right).

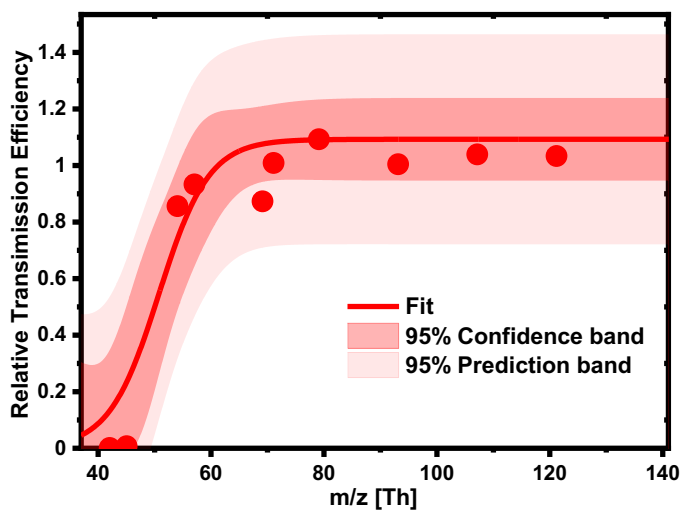


Figure S3 Relationship between relative transmission efficiencies of ions and their mass-to-charge ratios (m/z).

35

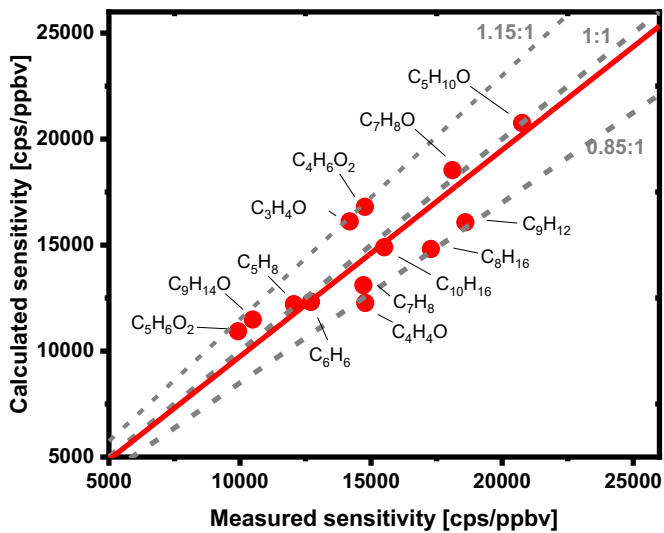
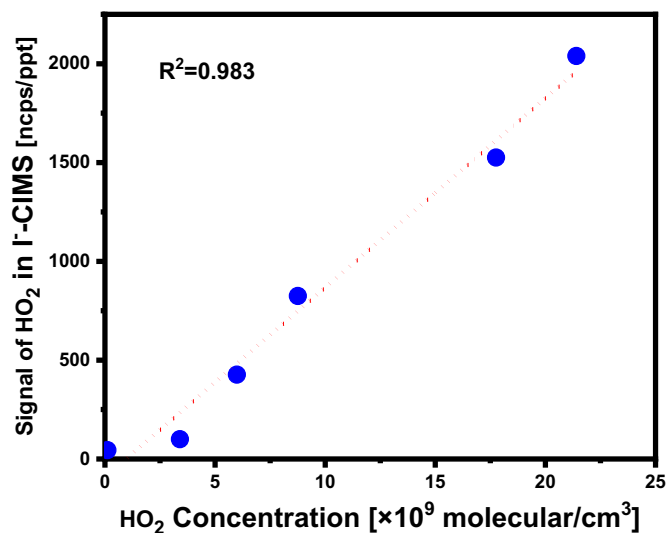
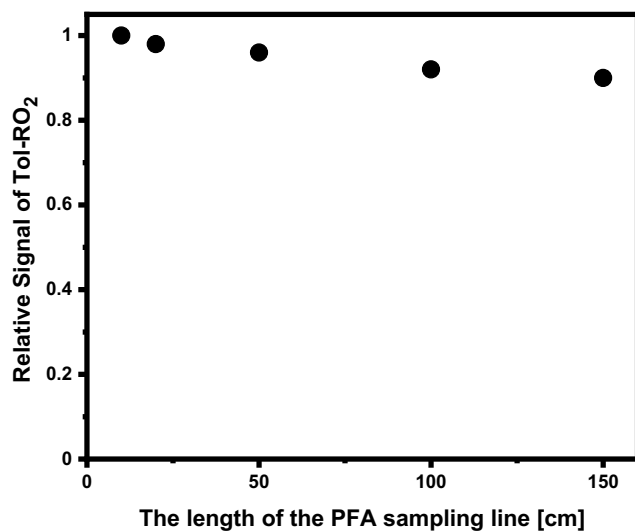


Figure S4 Comparison of calculated and measured sensitivities for different classes of compounds.



40 Figure S5 Calibration of the sensitivity of HO₂ radical by Vocus AIM

*: The concentration of HO₂ radicals was quantitatively determined utilizing LIF. Details about this instrument can be found in the previous reference(Wang et al., 2021).



45 Figure S6 Sampling loss assessment in PFA line (referenced to the signal at a line length of 0.1 m.

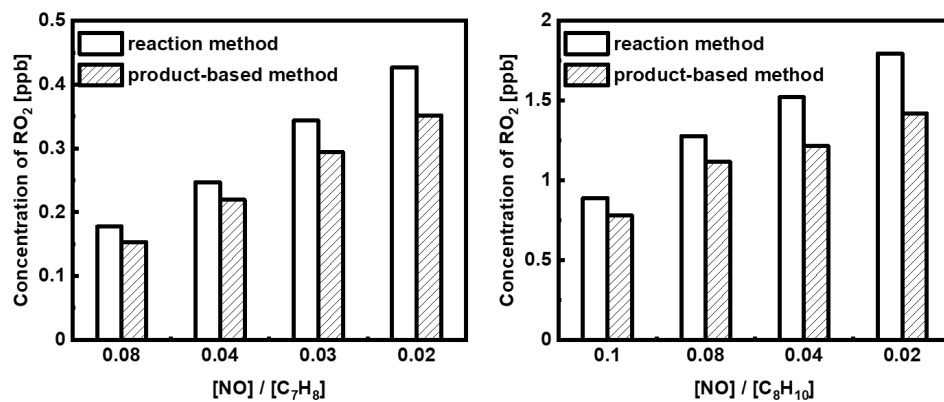


Figure S7 Comparison of RO₂ concentration in the calibrated system estimated using two methods in the oxidation of (left) toluene and (right) m-xylene.